applied sciences

MDPI

Article

A New Top-Mounted Shear-Hinge Structure Based on Modal Theory and Rubber-Pad Damping Theory

He En, Yuelei He *, Hongyao Lu and Anbin Wang

School of Urban Rail Transportation, Shanghai University of Engineering Science, Shanghai 201620, China
* Correspondence: hyldoc@163.com

Abstract: Steel-spring floating-slab tracks (SSFSTs) are widely used as efficient vibration-damping beds, and in China, they are mainly used in subways and municipal railroads. The shear hinge is an important component that improves the stability of the line, and field research has found that the top-mounted shear hinge (TMSH) undergoes varying degrees of damage, which indirectly affects the safety and stability of line operation. In this work, we studied the causes of damage to TMSHs, designed a new TMSH structure with a rubber-pad layer installed based on modal theory and rubber-pad vibration-damping theory, and proved that the new structure can reduce the occurrence of damage by comparing it with the original TMSH structure. The main aspects of this study are as follows: Firstly, the ultimate load capacity of the existing and new TMSH structures was checked by establishing a refined finite-element model. Then, modal analysis and frequency-response function analysis were carried out based on modal theory and frequency-response function theory to reveal the causes of TMSH damage and prove that the new structure can effectively delay damage. Finally, the modal and vibration patterns of the two structures were obtained via indoor hammering tests and compared with the simulation results. The results show that the two TMSH structures are in line with the strength requirements, and the existing TMSH damage mainly results from the resonance between its natural frequency and the high-excitation frequency of the floating slab under long-term cyclic train loading, causing high-frequency vibration fatigue damage. It is also demonstrated that the new structure can effectively reduce the natural frequency of the TMSH so that its value is located in the region of low vibration on the floating slab. The excitation vibration levels of the TMSH mounted on the curved section of the 4.8 m floating slab and the 3.6 m floating slab were reduced by 9 dB and at least 3 dB, respectively. After adding rubber pads located in the 400–3000 Hz floating-slab high-vibration-level region of the TMSH damage-prone parts, the amplitude reduction, including lateral excitation of damage-prone parts, resulted in a vibration amplitude reduction of more than 30 dB. However, the vertical excitation of the mid-end and rear-end bolts slightly increased their amplitudes, whereas the shear-rod amplitude was reduced by 48 dB, and the front-bolt amplitude was reduced by 5.28 dB. The natural frequency and vibration pattern obtained from the hammering test were consistent with the simulation results, and the reliability of our conclusions was verified from both experimental and simulation perspectives.

Keywords: top-mounted shear-hinge damage; modal analysis; frequency-response analysis; resonance; top-mounted shear-hinge structure optimization

check for updates

Citation: En, H.; He, Y.; Lu, H.; Wang, A. A New Top-Mounted Shear-Hinge Structure Based on Modal Theory and Rubber-Pad Damping Theory. *Appl. Sci.* **2023**, *13*, 8661. https://doi.org/10.3390/app13158661

Academic Editor: Suchao Xie

Received: 3 July 2023
Revised: 20 July 2023
Accepted: 25 July 2023
Published: 27 July 2023

Copyright: © 2023 by the authors. Licensee MDPI, Basel, Switzerland. This article is an open access article distributed under the terms and conditions of the Creative Commons Attribution (CC BY) license (https://creativecommons.org/licenses/by/4.0/).

1. Introduction

Steel-spring floating-slab tracks (SSFST) are one of the most successful types of tracks used in urban rail transportation worldwide, and their vibration-damping effect is globally recognized [1,2]. This is especially true in China, where urban rail transportation has developed rapidly in recent years, including subways, which are developing at a steady rate, and the new urban railroad, which is undergoing rapid development [3]. SSFSTs are used in large quantities and are composed of a rail, a floating slab, a steel-spring isolator, fasteners, and a shear hinge. SSFSTs are strong and discrete and therefore require the

installation of shear hinges to enhance the integrity of the bed, where the shear hinges, which connect the floating slabs, restrain the vertical and lateral differential movements of the slab ends [4]. Damage to different elements of SSFSTs under long-term train loading can directly affect the safety and stability of the SSFST system and vehicle operation [5–8]. As a structure that connects the floating slabs, the TMSH undergoes damage, such as loose and broken bolts and broken shear rods, during its service period. This damage accelerates fatigue damage to the fasteners and steel spring at the joint of the floating slab, which indirectly affects the service performance of the floating slabs and the railway. Thus, it is important to address the problem of damage to TMSHs in SSFSTs [9–11].

Of the few studies on shear hinges, most focus on the effects of the shear-hinge structure and structural parameters on the performance of floating-slab tracks. Chung et al. [12] set up a dowel joint, the earliest shear hinge, in an FST with an efficient joint model based on shear springs. They conducted vibration tests on the floating-slab track under four different working conditions regarding the installed positioning bar to study its effects on the load-transfer rate of the FST. The floating-slab track with the shear hinges installed was used to study the effect on the FST load-transfer rate and prove that the FST had good load-transfer capability after the installation of shear hinges. In addition, the accuracy of the finite-element model (FEM) model was verified through tests. Hussein et al. [13] also compared a shear hinge to a shear spring to study the effect of stiffness variation on the dynamic performance of a floating slab. Xu et al. [14,15] utilized a more complex shear spring to simulate a shear hinge to study the effect of a floating slab's length on its vibration response and the surrounding environment's vibration. Wei et al. [16] used a shear spring–dashpot model and a bending spring–dashpot model to simulate a shear hinge and compared the dynamic responses of the FST using two models. The authors demonstrated that both models could reduce the dynamic response of the floating slab. The above studies did not address the causes of damage to shear hinges or the measures that can be taken to address the damage. Moreover, they all used the shear spring or the spring–dashpot model to simulate shear hinges, which can only assess a shear hinge's performance from a single direction, and lack accuracy.

Since no research has been published on damage to top-mounted shear hinges, this paper will draw on the practices of other authors to analyze the causes of damage and optimize the design of their structure. Ma et al. [17] obtained the modal characteristics of fasteners under different preload assembly conditions through field tests, established a refined model of the fasteners, analyzed the dynamic characteristics of the elastic strips in the fasteners from both static and dynamic perspectives, revealed their fatigue damage mechanisms, specified the distribution characteristics of vulnerable points, and provided suitable values for the preloading of fasteners. Xiao et al. [18] established a fastener refinement model and performed static and dynamic analyses of the fastener sling under assembly conditions based on nonlinear contact theory. Their dynamic analyses mainly involved analyses of natural frequency vibration patterns and harmonious responses. Dynamic and static tests were conducted on a certain section of the line fastener, and the results showed that the insertion depth of the elastic strip was inadequate, resulting in resonance between the wave and wear-excitation frequency and the natural frequency, leading to the fracture of the elastic strip. Gao et al. [19] took high-speed rail fasteners as their research object and studied the relationship between wave wear, fastener dynamic characteristics, and fastener dynamic stress. They revealed the cause of fastener sling damage and designed a new damped sling to withstand high excitation frequencies and reduce the vibration peak. Through strength analysis and dynamic characteristics analysis, the authors proved that the new damped sling can effectively reduce the frequency response and cost. W. Dai et al. [20] investigated the effect of rubber-pad stiffness on the dynamic characteristics of a bridge deck plate using a transfer function, established a bridge model that considers continuous mass distribution in all directions, and analyzed the results obtained without an isolation pad and with different rubber shear moduli. It was shown that the rubber pads could effectively reduce the vertical natural frequency of the deck

plate, except for the fundamental frequency, but they had little effect on the horizontal natural frequency. Rubber-pad floating slabs are used extensively on subway lines [21–24], which proves that rubber can effectively reduce the vibration of floating slabs. The lower the stiffness of the rubber pad under the slab, the lower the natural frequency of the floating slab.

In summary, in this paper, we design a new rubber-pad shear-hinge structure based on modal theory and rubber-pad damping theory. The aim is to reduce the natural frequency of the top-mounted shear hinge to the vibration level of the excitation frequency of the floating slab's lower region, and at the same time, reduce the vibration amplitude of the region with a higher vibration level. The damaged area and damage rate of the TMSH structure during the operation are first determined using field survey results. Then, refined models of the existing TMSH and the new TMSH are established, and the ultimate load-carrying capacity of the two structures is verified by determining the SSFST and static equivalent train load. The dynamic characteristics of the two structures are studied, and the natural frequencies and vibration patterns of the TMSH in its assembled state are obtained based on preload modal theory. Frequency-response function analysis of the damaged parts of the TMSH found in the field survey reveals the causes of damage, and the natural frequencies and frequency-response function peaks of the two structures are compared and studied to prove the effectiveness of the new structure from a simulation point of view. The new structure is proven to be effective in lowering the TMSH's natural frequency, reducing the influence of floating-slab excitation and improving the TMSH's fatigue life from two perspectives.

2. TMSH Field Research

2.1. Basic Information on the Subway Line

To fully understand the status and performance of the shear hinge in actual operation, field research was conducted on an old subway line that had been in operation for 13 years and on a new line that had been in operation for 2 years, with speeds of 70–80 km/h. It is known that there are three different types of shear hinges: the top-mounted shear hinge (TMSH), side-mounted shear hinge (SMSH), and built-in shear hinge (BISH). The types of shear hinges used on the old line and the new line are the TMSH and SMSH. The old line comprises a 4.8 m prefabricated steel-spring floating-slab track, with DTIII2-type fasteners used to fix the rail. The shear-hinge layout combines a TMSH and an SMSH, as shown in Figure 1. The TMSH is pinned into a sleeve, and an M24 bolt fixes it to the adjacent two floating slabs, symmetrically along the track centerline, positioned on the outer side of the rail.

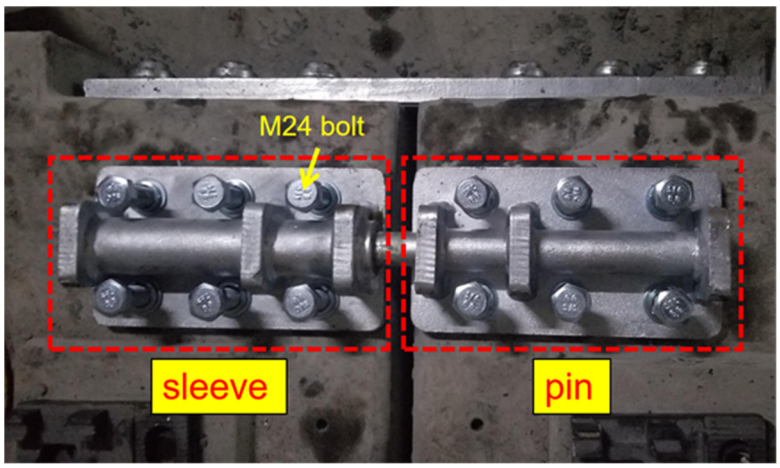

Figure 1. Structural diagram of the old line's TMSH.

The new line comprises a 3.6 m prefabricated steel-spring floating-slab track with a WJ-2 fastener and uses a double-TMSH layout, as shown in Figure 2. Two pairs of shear

hinges are symmetrically positioned on the inner and outer sides of the rail. In Figure 2, it can be seen that the shear hinge of line 15 is composed of a sleeve, a shear rod, and M24 bolts. According to field research, TMSHs have various shapes, but the working principle is always the same, so the effect of the shape of the TMSH on its performance is not considered in this study.

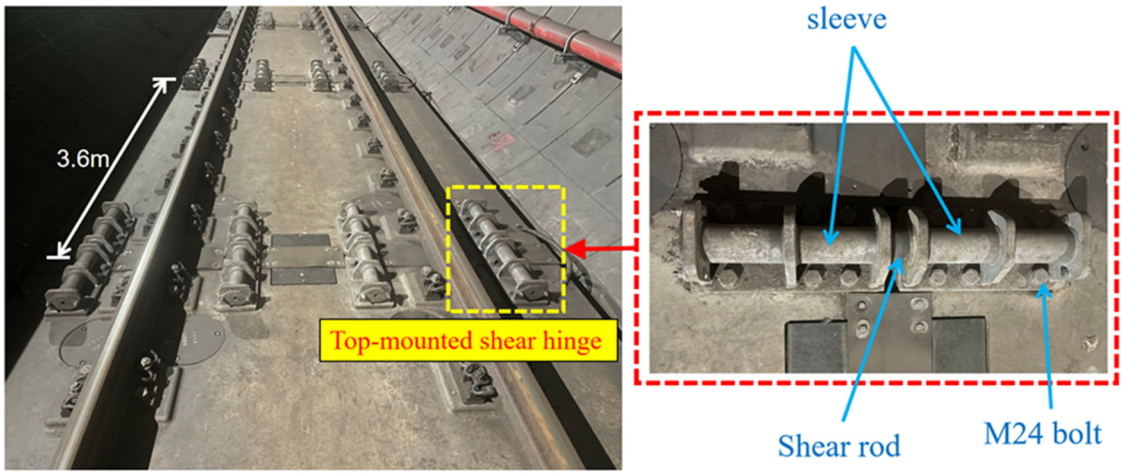

Figure 2. Structural diagram of the new line's TMSH.

2.2. Damage to the TMSH

Through field research to examine the old and new lines, respectively, we found that the TMSH-to-SMSH ratio was 3:1, and SMSHs did not incur damage. In the TMSHs, we found bolt loosening, broken bolts (Figure 3), pin or shear-rod fracture (Figures 4 and 5), and other types of damage, as shown in Table 1.

In the table, it can be seen that the damage to the TMSH was mainly concentrated in the curved section, but after long-term operation, the straight section also had some damage. The loose-bolt problem occurred more frequently compared to other problems, and no broken-bolt or shear-rod fracture problems were found in the straight-line section of the new line.

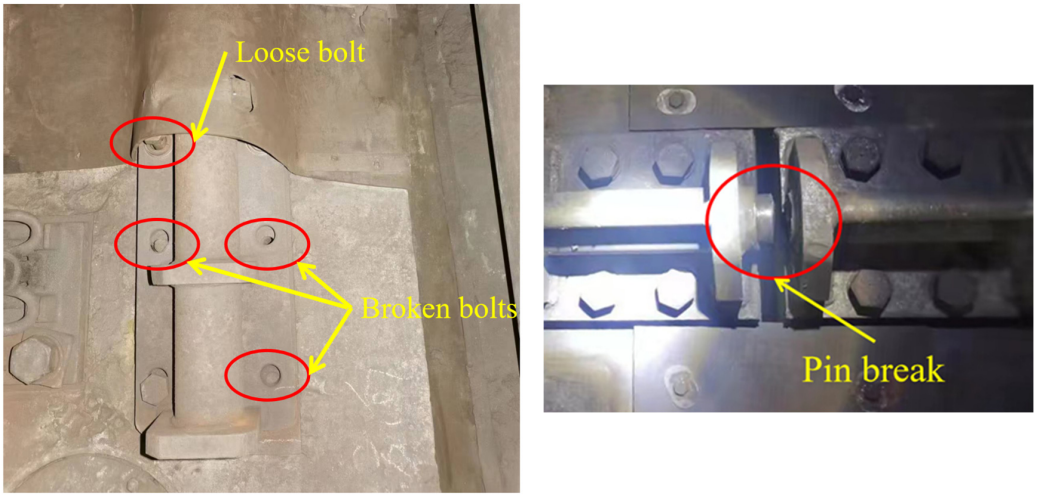

(**a**) (**b**)

Figure 3. *Cont.*

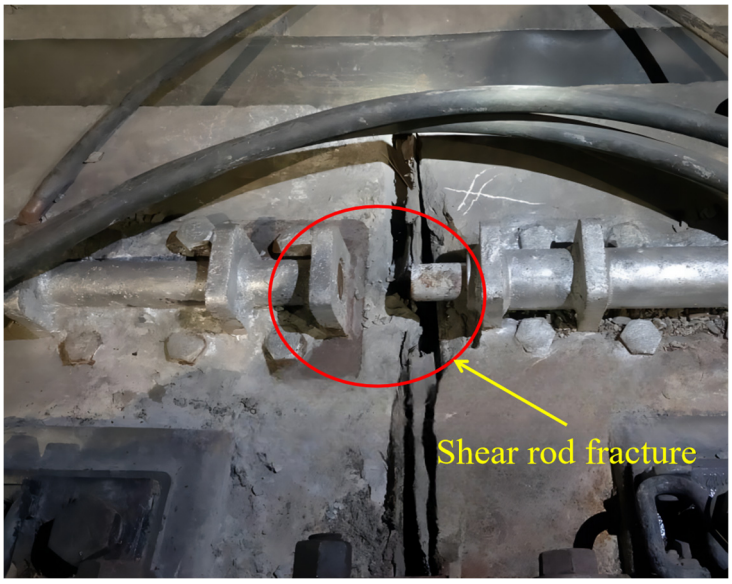

(**c**)

Figure 3. Shear-hinge damage during field research: (**a**) loose bolts and broken bolts, (**b**) pin fracture, (**c**) shear-rod fracture.

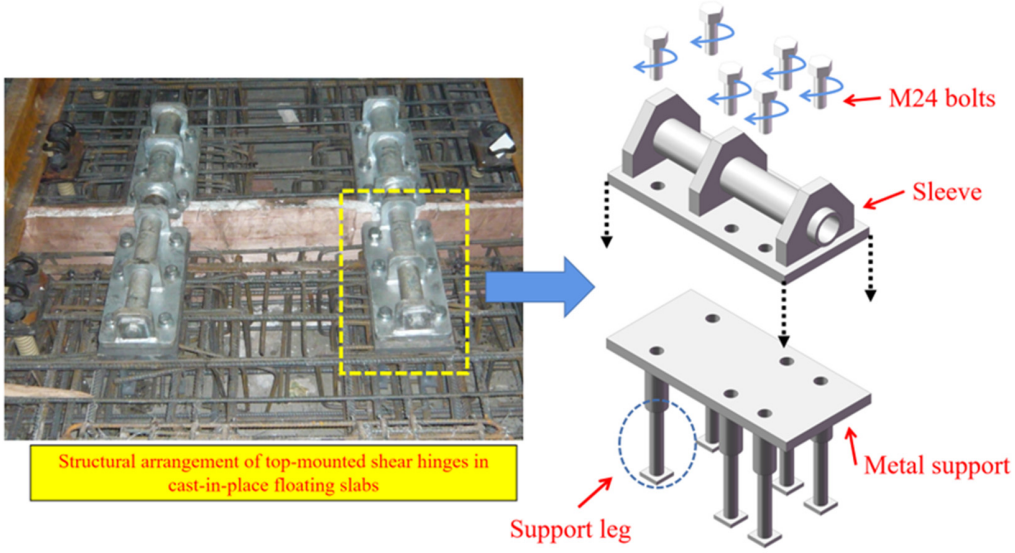

Figure 4. Full view of the TMSH structure during the site survey.

Table 1. Statistics of shear-hinge damage observed in field research.

Line Type	Loose Bolts		Broken Bolts		Pin or Shear-Rod Fracture	
	Quantity (pcs)	Percentage (%)	Quantity (pcs)	Percentage (%)	Quantity (pcs)	Percentage (%)
Old line straight	20	4.4	2	0.4	1	2.6
Old line curved	31	6.8	10	2.2	3	7.9
New line straight	16	1.8	0	0	0	0
New line curved	48	5.3	11	1.2	2	2.6

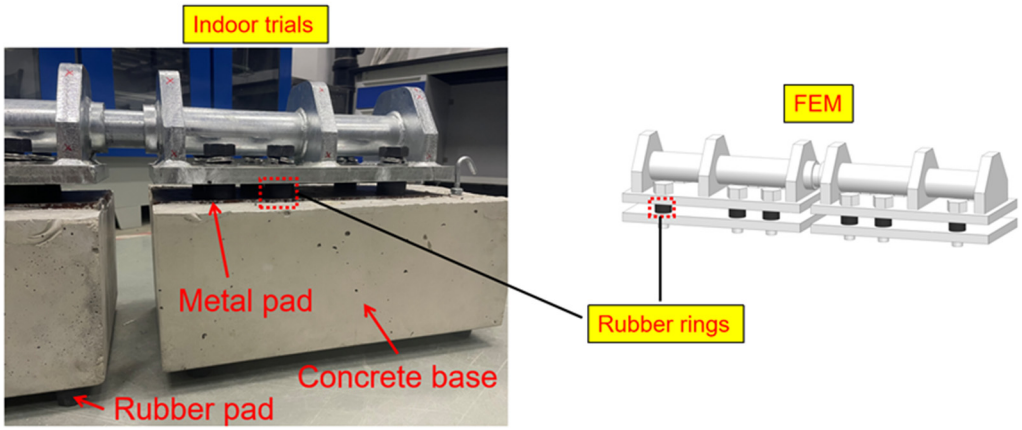

Figure 5. Design of new TMSH structure.

2.3. Analysis of the Causes of Damage to the TMSH

It was presumed that the current design of the shear-hinge structure has some problems. Upon observing the prefabricated floating slab before concreting the shear-hinge structure, as shown in Figure 4, it was found that the TMSHs were installed directly on the metal pad using M24 bolts, and the metal pad was fixed to the reinforcement through the support leg when the steel cage of the prefabricated floating slab was made, which was fixed to the floating slab with concrete. The overall structure did not contain vibration-isolation pads or other vibration-damping measures, resulting in the high-frequency vibration response of the train load on the floating slab being transferred directly to the shear hinge. This excited the modal frequency of the shear hinge and caused structural resonance, which then led to damage. Therefore, the preliminary judgment is that inadequate structural design is one of the main reasons for pin or shear-rod fracture, bolt loosening, and broken bolts in the TMSH.

2.4. Structural Design Optimization

As a highly elastic material with good vibration damping and low cost, rubber is widely used in subway lines, including for rubber floating-slab tracks [23], typical rubber-to-metal bonded components for rail suspension systems [25], and new vibration isolators that combine the particle damping and vibration absorption of rubber materials with bandgap vibration resistance [26]. The shear hinge is mainly subjected to vibration from the floating slab in the vertical direction during service, so only the vertical degree of freedom of the shear hinge is considered. The shear hinge's natural frequency can be expressed as:

$$f = \frac{1}{2\pi}\sqrt{\frac{k}{m}} \tag{1}$$

The formula for calculating the vertical-support stiffness of the rubber bearing is as follows [27]:

$$K_{v=}\frac{E_{cb}A}{nt_r} \tag{2}$$

where $K_v(k)$ is the vertical-support stiffness, E_{cb} is the modified elastic compression modulus, A is the effective cross-sectional area of the support, n is the number of rubber pads, and t_r is the thickness of the rubber pad.

$$E_{cb} = \frac{1}{E_c} + \frac{1}{E_b} \tag{3}$$

$$E_c = E_0\left(1 + 2\kappa S_1^2\right) \tag{4}$$

where E_c is the longitudinal modulus of elasticity of rubber under pure compression, E_b is the bulk modulus of elasticity of rubber, κ is the rubber hardness correction factor (the specific values are given in [28]), and S_1 is the primary shape factor (S_1 = D/4t_r). After measurement, the total weight of the TMSH is 60.34 kg, and the parameters of the rubber pads are shown in Table 2. In order to reduce the natural frequency of the TMSH to the low-vibration region of the floating slab, the target frequency is set to 80 Hz (in Figure 17b,d of [29], it is shown that the low-vibration region of the floating slab will be entered after 80 Hz), and Equations (1)–(4) are then substituted to calculate the results. Twelve ring-shaped rubber pads with an inner diameter of 24 mm, an outer diameter of 48 mm, and a thickness of 18 mm are supported through the bolts between the shear hinge and the metal pad to reduce the natural frequency of the TMSH, as shown in Figure 5.

Table 2. Sensor parameters.

IRHD	E_0/MPa	κ	E_∞/MPa	n
70	7.34	0.53	1270	1

Due to the long-chain molecular structure of rubber and the small secondary force between molecules, it has viscoelastic properties and can absorb the vibration load transmitted from the floating slab. It is believed that rubber pads can attenuate the vibration through inertial motion and then transmit it to the shear hinge so that the natural frequency of the shear hinge can withstand the peak vibration frequency of the floating slab. It is expected that this can reduce the vibration level of the shear hinge.

3. Finite-Element Modeling

3.1. TMSH Model

In this paper, we perform research based on the TMSH of a sleeve-shear-rod structure. We then build models of each component using SOLIDWORKS, assemble them, and import them into ABAQUS. Since the structure is an assembly, the meshes of the shear rod and sleeve parts need to be seeded and undergo layout processing to achieve the desired effect. To simplify the model, the support leg used to fix the metal pad is ignored. The metal pad layer, the shear rod, and the M24 bolts are located on the surface in the contact setting, so a grid encryption process is carried out for them. All cells in this model are solid cells, and the sleeve, shear rod, metal pad, and M24 bolt grid cells are defined as C3D8R, which can overcome the self-locking problem. The rubber pad with incompressible properties is defined as a hybrid single C3D8RH.

3.2. Material Properties, Constraints, and Load Settings

The TMSH material is 60Si2Mn. According to the literature [17], the 60Si2Mn's modulus of elasticity is 201 GPa, its yield strength is 1293 MPa, and its fracture strength is 1430 MPa. A bilinear reinforced intrinsic structure model is used to define the mechanical parameters of the TMSH, and the material properties of the metal pad are the same as those of the TMSH. In the actual process of using rubber, its deformation is very small, and the displacement caused by the TMSH is much smaller than its size, so to simplify the model, a linear stress–strain curve is used instead of the superplastic rubber intrinsic model [30]. The specific parameters of the material are shown in Table 3, where the rubber has a natural hardness of 40.

Table 3. Material parameters of TMSH.

Material	Young's Modulus/Pa	Poisson's Ratio	Density kg/m^3
60Si2Mn	2.01×10^{11}	0.29	7850
Rubber	1.5×10^{6}	0.4995	1300

The TMSH is connected to the bolt sleeves cast in the floating slab using bolts. To facilitate the calculations, the strength of the TMSH is verified by default with intact TMSHs, i.e., the bolts are connected to the floating slab via a fixed connection. In the modal analysis of the TMSH, to simulate real contact in the field, the normal interaction property is defined as hard contact when setting the contact properties of each component to prevent the models from penetrating each other. Additionally, the tangential interaction is defined as a penalty function friction model, the friction coefficient between the metals is set to 0.2, and the friction coefficient between the metal and rubber is 0.7. In order to increase the model convergence, the enhanced Lagrangian algorithm is used for the vertical contact between the shear rod and the two bushings, and between the rubber and the metal (in order to save computational effort, the contact between the shear rod and the bushings is set as a fixed constraint during the strength check), and all the bottom surfaces are set as fixed constraints. According to the requirements of a city subway line, the shear-hinge bolt torque is 300 N·m, and the TMSH M24 bolt diameter is 24 mm, according to the following formula [31]:

$$F_{bolt} = \frac{M_{bolt}}{0.17 d_{bolt}} \tag{5}$$

where F_{bolt} is the bolt preload force, M_{bolt} is the bolt torque, d_{bolt} is the diameter of the bolt (calculated using Equation (5)), and the corresponding bolt preload is 73.529 kN. The TMSH loads and constraints are shown in Figure 6.

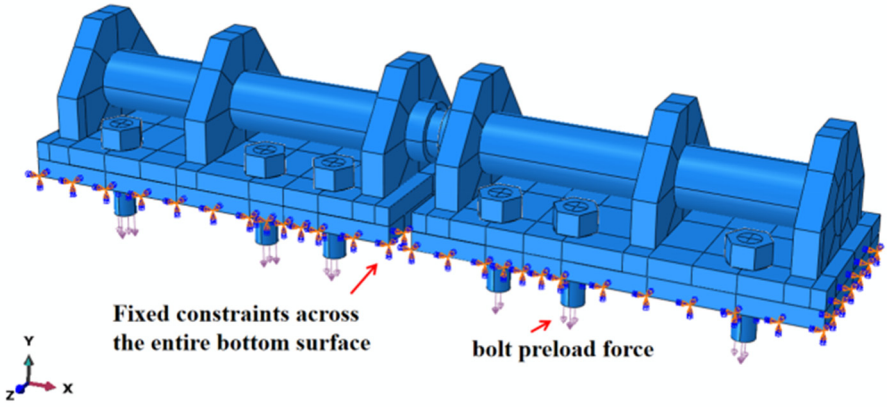

Figure 6. TMSH constraints and loads during modal analysis.

3.3. TMSH Strength-Check Calculation

To verify the load-carrying capacity of the TMSH structure and ensure that it conforms to the ultimate load range under the most unfavorable operating conditions, the Mises stress criterion [32] of the fourth strength theory, i.e., the distortional energy density theory, is introduced to calibrate the shear-hinge strength, which is mainly calculated from the principal stresses in three directions using Equation (6).

$$\sigma = \sqrt{\frac{1}{2}\left[(\sigma_1 - \sigma_2)^2 + (\sigma_2 - \sigma_3)^2 + (\sigma_3 - \sigma_1)^2\right]} \tag{6}$$

In the above formula, σ represents the Mises stress, and σ_1 , σ_2, and σ_3 represent the first, second, and third principal stresses, respectively. Strength theory suggests that if the distortion energy density reaches a certain limit related to the material properties, the material will yield.

The establishment of the floating-slab shear-hinge refinement model is shown in Figure 7. To save computing resources and ensure the authenticity of the calculated structure as far as possible, the validation model establishes a three-link refined floating-slab structure, with TMSHs and SMSHs using refined models, and rails simulated using Timoshenko Beam B21. In order to prevent rail deformation from influencing the results, rail

stiffness is calculated according to the material properties, and fasteners and steel-spring isolators are simulated using Connector, as shown in Table 4.

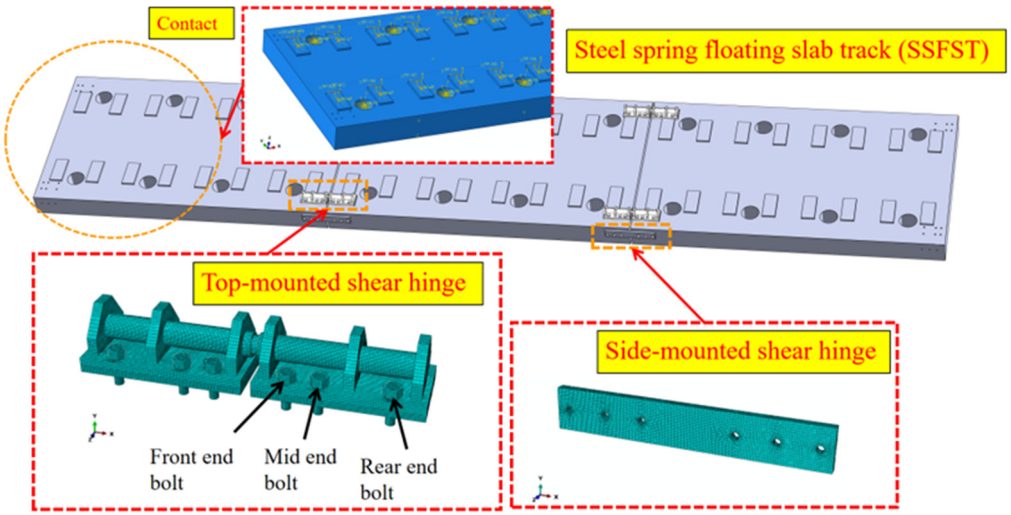

Figure 7. Strength-verification model of TMSH.

Table 4. Floating-slab model parameters.

Component	Parameter	Value
Prefabricated floating slab	Floating-slab size	4.776 m × 2.7 m × 0.35 m
	Young's modulus	34,500 MPa
	Density	2500 kg/m^3
	Poisson's ratio	0.2
Steel-spring isolator	Vertical stiffness	60×10^6 N/m
	Lateral stiffness	7×10^8 N/m
	Vertical damping	12,000 N × s/m
	Layout distance	1.2 m
Fastener	Vertical stiffness	3×10^7 N/m
	Lateral stiffness	1×10^7 N/m
	Vertical damping	10,000 N × s/m
Rail	Mass	60.64 kg/m
	Young's modulus	2.01×10^9 Pa

When a train runs on a floating slab, the internal forces on the track components caused by wheel loads can be equated to those caused by static loads. Taking Metro A as the standard, each bogie is equipped with two-wheel pairs for a total of four wheels, with a wheel spacing of 2.5 m and a single axle weight of 16 t. According to the description given in Appendix F (Track-Strength Verification) in the Code for the Design of Railway Tracks [33], the dynamic wheel load is expressed as the maximum possible value of the equivalent static load. The equivalent vertical static load is calculated as follows:

$$\begin{cases} v \le \frac{120\ \text{km}}{h} & P_d = P_o(1+\alpha) \\ \frac{120\ \text{km}}{h} < v \le \frac{160\ \text{km}}{h} & P_d = P_o(1+\alpha)(1+\alpha_1) \end{cases} \tag{7}$$

where P_d is the vertical equivalent static load of the wheel acting on the rail, P_o is the static wheel weight, V is the travel speed, and α, α_1 is the speed coefficient.

$$\alpha = 0.6v/100 \tag{8}$$

$$\alpha_1 = 0.3\Delta v_1/100 \tag{9}$$

The average speed of operation on the straight section is 80 km/h, and the axle weight of the train is multiplied by 1.48 coefficients. When the bearing capacity of the floating slab is checked, the axle weight of the train is also multiplied by 1.4 sub-coefficients. The gravity coefficient is taken as 9.8 m/s^2 and substituted into Equations (7)–(9) to calculate $P_d = 162.4$ (kN).

The curved section is a shear-hinge damage-prone section so the strength of the shear hinge on the curved section is calibrated by considering the lateral load. The lateral load of the train is determined by the static wheel weight, derailment coefficient, and wheel–rail friction coefficient μ_k. The load of a train wheel pair with only one wheel rim and rail transverse contact that produces a transverse force is calculated as the value of the static wheel weight multiplied by the derailment coefficient. For the other wheel with the wheel tread and rail top contact, the load is calculated as the maximum transverse force of the static wheel weight multiplied by the dynamic friction coefficient. The derailment coefficient is 0.8, and the dynamic friction coefficient is 0.2. The larger value of transverse force is calculated using Equations (7)–(9) to be 64 kN, and the transverse force on the other side is 16 kN.

Since three floating-slab tracks are built in this validation model, only the adjacent bogie loads of two adjacent carriages are considered, and the load is applied using 1/2 fastener spacing as the step length, running uniformly and continuously along the x-axis. Figure 8 shows the stress value of the shear rod under metal-pad conditions, with a maximum strength of 180.9 MPa, and Figure 9 shows the stress values with an additional rubber-pad layer. The shear rod is subjected to a maximum Mises stress value of 150.9 MPa. From a static point of view, the rubber pad reduces the stress value of the shear rod by 16.7%.

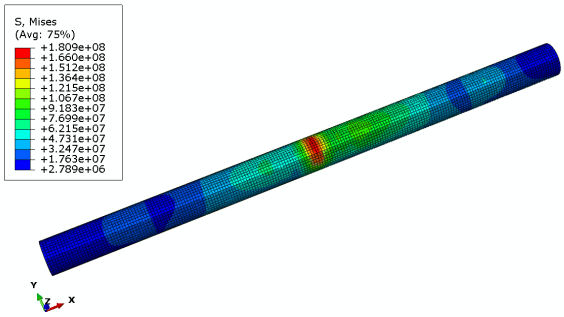

Figure 8. Shear-rod stress values for top-mounted shear hinges mounted on metal pads.

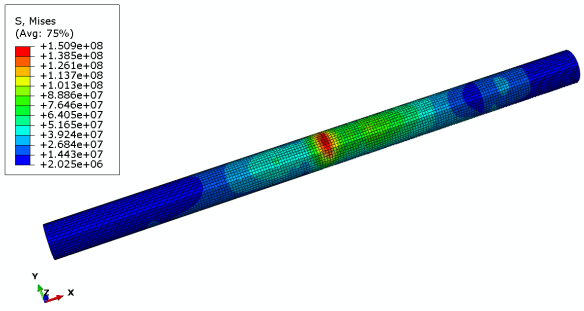

Figure 9. Shear-rod stress values for top-mounted shear hinges mounted on rubber pads.

According to the material definition, the yield strength of the 60Si2Mn used in the shear hinge is 1293 MPa. Taking a safety factor of 2, the permissible strength stress is calculated as follows:

$$[\sigma] = \frac{\sigma_b}{n} \tag{10}$$

where σ_b is the material yield strength, n is the safety factor, and the calculated permissible stress is 646.5 MPa. $[\sigma_{max}] < [\sigma]$ under the two operating conditions, which is fully compatible with user requirements.

4. Modal Analysis and Frequency-Response Analysis under Assembly Conditions

According to the field research, the damage to the current shear hinge mainly consisted of a shear-rod break, bolt loosening, and broken bolts. Pre-stress application will change the structural-stiffness matrix, so to obtain the natural frequency of the shear hinge's working conditions, a shear-hinge pre-stress assembly modal analysis was conducted. The natural frequencies are shown in Figure 10, and the vibration patterns are described in Table 5 (the displacements in the results do not have any physical meaning and are not exact displacements; they are only used to determine the direction of vibration). We used the pre-stressing modal method for nonlinear modal analysis of the shear-hinge assembly. In the second step, a modal analysis step was established using the Lanczos method to extract the 20th mode and solve the vibration equation.

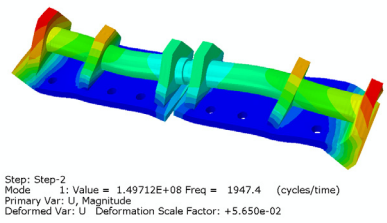

First-order mode (1947.4 Hz)

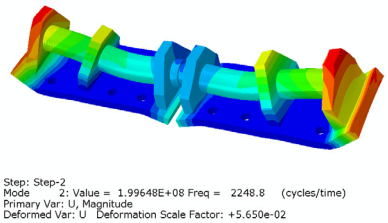

Second-order mode (2248.8 Hz)

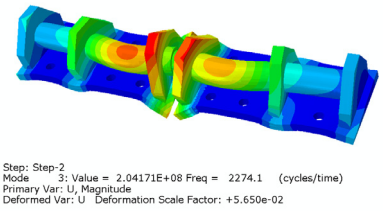

Third-order mode (2274.1 Hz)

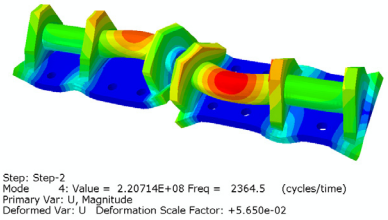

Fourth-order mode (2364.5 Hz)

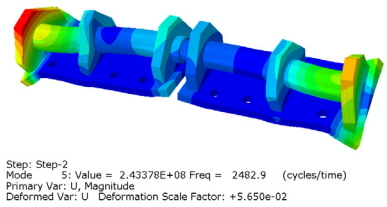

Fifth-order mode (2482.9 Hz)

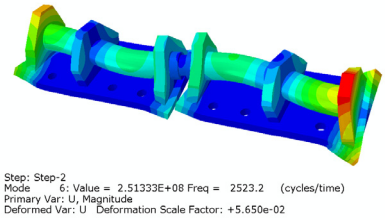

Sixth-order mode (2523.2 Hz)

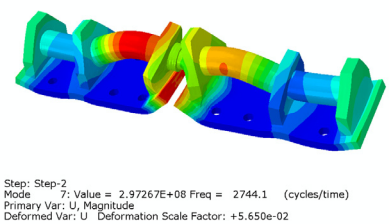

Seventh-order mode (2744.1 Hz)

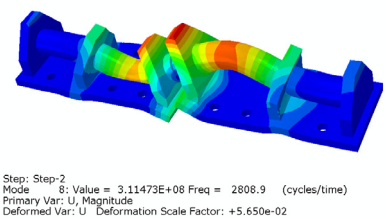

Eighth-order mode (2808.9 Hz)

Figure 10. Natural frequency when the TMSH is placed on the metal pad.

Table 5. Description of vibration pattern when TMSH is placed on metal bedding.

Order	Frequency/Hz	Description of the Vibration Mode
First	1947.4	First-order bending, front and rear sleeve warping at the opposite end, asymmetric bending of the shear rod, large amplitude at the rear end
Second	2248.8	Second-order bending, front and rear of sleeve warped at the same end, shear rod bent symmetrically, large amplitude at the rear end
Third	2274.1	First-order torsion, both ends of the sleeve along the shear rod undergo axial counterclockwise rotation, the front amplitude is large
Fourth	2364.5	Second-order torsion, both ends of the sleeve along the axial axis of the shear rod undergo clockwise rotation, the front-end amplitude is large
Fifth	2482.9	Third-order torsion, both sides of the sleeve along the shear rod undergo axial anisotropic rotation, both ends of the sleeve undergo anisotropic rotation, the rear end amplitude is large
Sixth	2523.2	Fourth-order torsion, both ends of the sleeve along the axial direction of the shear rod undergo counterclockwise rotation, both ends of the sleeve undergo the same direction of rotation, the rear end amplitude is large
Seventh	2744.1	Third-order bending, front and rear of sleeve warped at the same end, shear rod bent symmetrically, large amplitude at the rear end
Eighth	2808.9	Fourth-order bending, front and rear of sleeve warped at opposite ends, asymmetric bending of the shear rod, large amplitude at the rear end

4.1. Analysis of TMSH Modalities When Using a Metal Pad

As shown in Figure 10, the first-order mode of the shear hinge was 1947.4 Hz and its natural frequency was mainly concentrated in the middle-to-high range, with reference to the peak frequency range of floating-slab vibration [34]. Prefabricated steel-spring floating slabs of 4.8 m and 3.6 m were tested for indoor hammer shock vibration, and one-third-octave diagrams were obtained (Figure 17a,b). The vibration acceleration of straight and curved sections of SSFSTs in operation has been tested in the literature [29]. According to the one-third-octave diagrams (Figure 17b,d), the high-frequency amplitude decreased with increasing frequency, so this paper focused on mode oscillations with natural frequencies below 3000 Hz.

The TMSH itself is located at the connection of the floating slab and is subjected to transverse and longitudinal shear forces when a train passes through it. A resonance phenomenon occurred when the natural frequency obtained from the modal analysis of the TMSH assembly coincided with the high-excitation frequency of the floating slab.

4.2. Analysis of TMSH Modalities When Using a Rubber Pad

According to the new structure proposed in Section 2.4, the rubber gasket is placed between the TMSH and the metal pad, and the modal calculation results are shown in Figure 11, and the vibration patterns are described in Table 6.

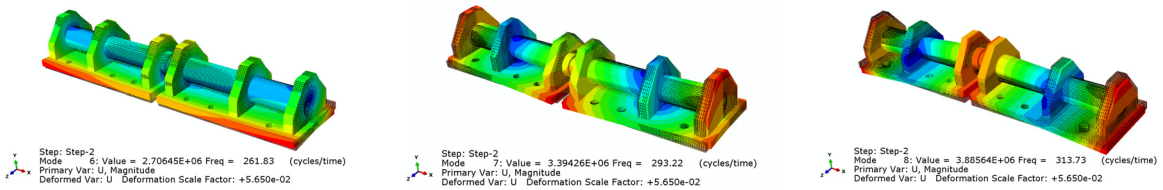

First-order mode (261.83 Hz) Second-order mode (293.22 Hz) Third-order mode (313.73 Hz)

Figure 11. Natural frequency when TMSH is placed on the rubber pad.

Table 6. Description of the vibration pattern when the TMSH is placed on the rubber pad.

Order	Frequency/Hz	Description of the Vibration Mode
First	261.83	The TMSH is rotated along the *x*-axis and slightly bent along the *z*-axis.
Second	293.22	The TMSH is bent along the *z*-axis
Third	313.73	The TMSH is bent along the *y*-axis

Only the third-order-mode TMSH was found to occur in vibration mode. According to the theoretical calculation, the natural frequency of the new structure should be about 100 Hz, but the first few orders of vibration-mode panning are mostly considered to be false, so they were not considered. A mode of more than 313 Hz on the TMSH is considered weak, so the third-order mode was extracted. It can be seen in Table 7 that the TMSH's natural frequency decreased significantly after adding the rubber pad, and the average modal improvement rate was 86–87%, which proves that the rubber pad can effectively reduce the TMSH's natural frequency. According to the results, the TMSH's natural frequency after the installation of the rubber pad was in the operating low-frequency region of 250–315 Hz for the floating slab. According to the currently available data [29], four different working conditions were established, as shown in Table 8, which lists the differences in vibration levels when the TMSH was placed on the rubber pad and the metal pad, respectively. Moreover, the magnitudes of the vibration levels were compared when the TMSH's natural frequency coincided with the excitation frequency of the SSFST before and after the addition of the rubber pad, and the results are shown in Figure 12.

Table 7. Comparison of the shear force before and after the addition of rubber pads in relation to the natural frequency of the structure.

Order	Metal Pad	Rubber Pad	Modal Improvement Rate
First	1947.4	261.8	86.6%
Second	2248.8	293.2	87%
Third	2274.1	313.7	86.2%

Table 8. The differences in vibration levels between TMSHs with and without rubber pads under four working conditions.

Working Conditions	Drop-Hammer Impact Test—3.6 m	Drop-Hammer Impact Test—4.8 m	Straight-Line Vibration Test—SSFST	Curved-Line Vibration Test—SSFST
Serial number	1	2	3	4
dB difference/dB	3	9	−8	9

In Figure 12 and Table 7, it can be seen that the vibration levels increased considerably from Case 2 to Case 3, which is due to the fact that Case 1 and Case 2 represent the results of the hammer test conducted indoors, whereas Case 3 and Case 4 represent the field measurements of the running line, and the field excitation was larger compared to the hammer excitation indoors. Meanwhile, it can be seen that the vibration level of the TMSH after adding the rubber pad was lower compared to that of the structure without the TMSH, except in the vibration test of the linear section. Moreover, the vibration levels at the location of the natural frequency under the other three working conditions were reduced, with the vibration levels of working condition 2 and working condition 4 reduced by 9 dB, and the vibration level of working condition 1 reduced by 3 dB. This proves that the installation of the rubber pad can effectively reduce the vibration level of the TMSH in the curved sections of the 4.8 m floating slab and 3.6 m floating slab. It is proven that the installation of rubber pads can effectively reduce the vibration levels of the 4.8 m floating slab and the 3.6 m floating slab when the TMSH's natural frequency and the excitation frequency of the floating slabs coincide so that the amplitude under the cyclic load is reduced and the fatigue-damage time is slowed down.

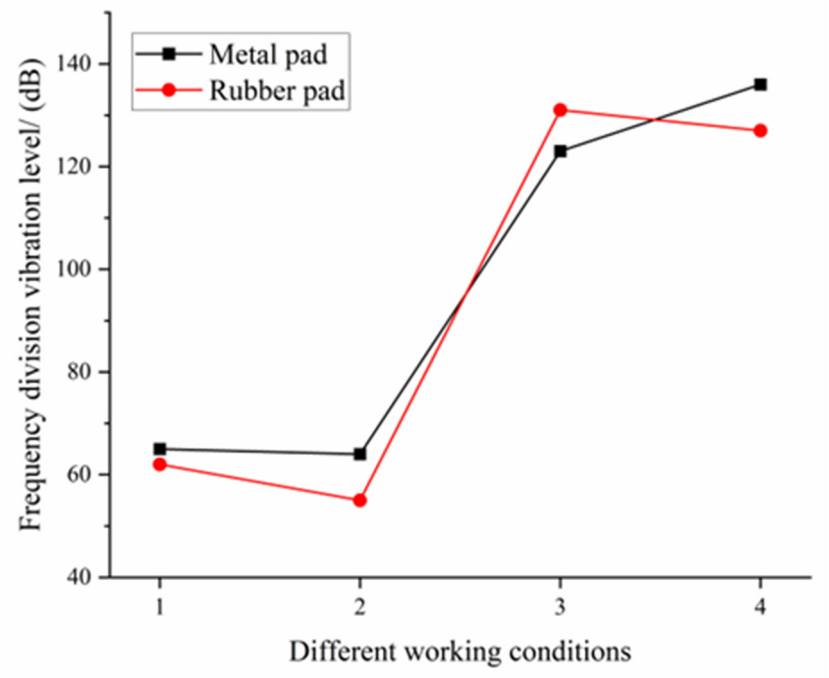

Figure 12. Comparison of vibration levels under four operating conditions before and after adding rubber pads to the shear hinge.

4.3. Analysis of Shear-Hinge Frequency-Response Function When Metal Padding Is Added

To further investigate the resonant frequency of the TMSH installation state, frequency-response analysis was performed on the TMSH. According to the peak of the excitation frequency of the floating slab, the sweeping frequency range was determined to be 20–3000 Hz for sinusoidal excitation, and the vibration amplitude was extracted when the steady state was reached. It was found that the modal vibration pattern had a certain symmetry along the longitudinal direction. Considering the damage found during the field research, the frequency-response function curves of a total of four damage-prone areas under vertical and transverse load excitations were extracted from the connection between the shear rod and the sleeve, and the root of the head of the front, middle, and rear three bolts (see figure for definition), respectively. The extraction results are shown in Figure 13.

Using the resonance peak position of the frequency-response function curve, as shown in Figure 13a, it was found that the shear rod connected with the sleeve was more sensitive to transverse excitation near the second order (2184 Hz), and it was observed that the modal vibration pattern of this order had some influence on the connection between the shear rod and the sleeve. In Figure 13b, it can be seen that under the vertical excitation of the floating slab, the shear rod had a resonance peak in the third order (2265.5 Hz), a resonance peak existed near the seventh order (2710.2 Hz), and the acceleration admittance at 2689.2 Hz was six times higher compared to that at 2253.5 Hz. The third-order vibration pattern mainly manifested as twisting of the front end of the shear hinge and reverse bending of the shear rod, and the seventh-order vibration pattern was characterized by the bending and buckling of both ends of the sleeve, which also caused bending of the shear rod in the opposite direction to the sleeve's bending direction. Based on this, it can be speculated that under long-term cyclic high-frequency excitation, the second order, the third order, and, especially, the seventh order may cause the shear rod to develop cracks and eventually fracture.

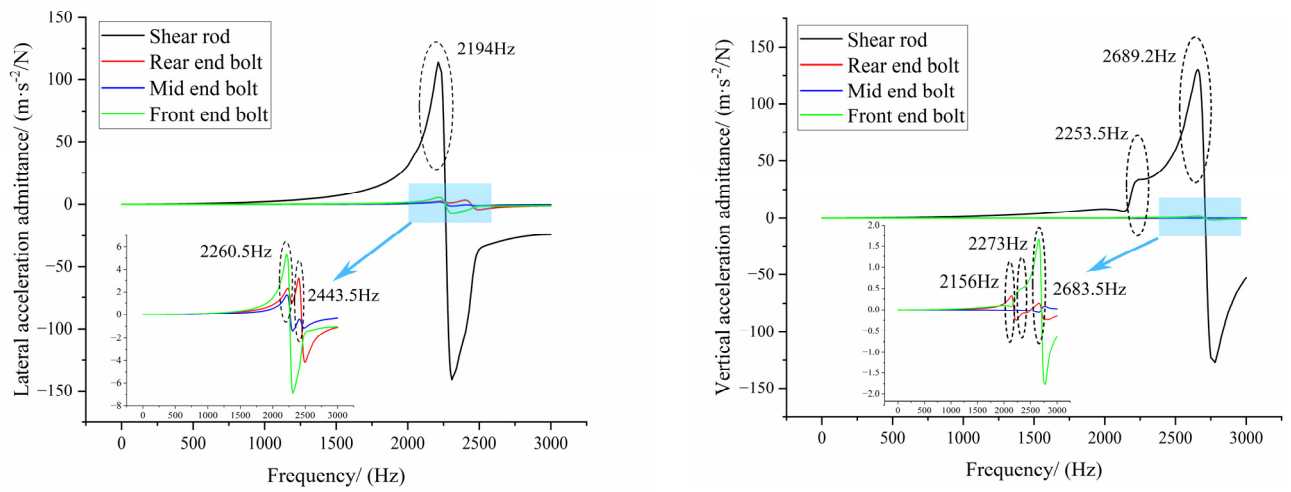

(**a**) (**b**)

Figure 13. Vertical and lateral frequency-response analysis results for TMSH installed on the metal pad: (**a**) lateral acceleration admittance; (**b**) vertical acceleration admittance.

Compared with the shear rod, the effect of external excitation on the bolt was small, but there were multiple resonance peaks. Figure 13a shows that the front-end, middle-end, and rear-end bolts all had resonance peaks at 2260.5 Hz during lateral excitation, i.e., the third order (2265.5 Hz), and this order frequency had a greater effect on the front-end bolt. The rear-end bolt and middle-end bolt had resonance peaks at 2443.5 Hz, i.e., a peak also appeared in the fifth-order mode (2444.5 Hz), and this order mode's rear-end bolt response was greater compared to that of the third-order mode. In the middle-end bolt, despite having a resonance peak in both mode orders, compared to the front-end and rear-end bolts, its peak was not obvious. In the vertical excitation of the front-end bolts in the third order and the seventh order, there were two resonance peaks. The seventh-order peak was higher, the rear-end bolts in the second-, third, and seventh-order modes had weak resonance peaks, and the middle-end bolts were not excited. The front-end bolt was prone to damage in the third-order mode and seventh-order mode, the middle-end bolt was prone to damage in the third-order mode, and the rear-end bolt was prone to damage in the second-order mode and fifth-order mode.

In summary, under train-load excitation, the TMSH's natural frequency resonates with the high-excitation frequency of the floating slab, and the resonant frequency intensifies the fatigue striations generated during the actual vibration process. This eventually accelerates the rate of fatigue fracture of the member from high-frequency vibration, which, in turn, leads to broken bolts and shear-rod fracture problems in the TMSH. The third- and fifth-order transverse vibrations to the bolt are the main cause of bolt loosening. Combined with the vibration level of the floating slab and the analysis of field research, the first few orders of natural frequency are more likely to cause damage to the curved section because the vibration level of this section is gradually reduced from 2000 Hz to 3000 Hz.

4.4. Analysis of Shear-Hinge Frequency-Response Function When Rubber Padding Is Added

In Section 4.2, it was demonstrated that the TMSH assembly's natural frequency is significantly reduced by adding a rubber bedding layer between the metal pad and the TMSH. In this section, the frequency-response function of the TMSH with rubber padding is analyzed, and the following figures show the frequency-response function curves of the TMSH's damage-prone areas.

In Figure 14a, it can be seen that the sensitive peaks of transverse acceleration admittance at the connection point of the shear rod and sleeve are near the first (261.83 Hz)- and second (293.22 Hz)-order modes and the peak level is higher in the first order. In

Figure 14b, it can be seen that the shear rod has only one sensitive peak under vertical excitation, which is located near the third-order (313.73 Hz) mode. The peak transverse acceleration admittance values of the front-, middle-, and rear-end bolts are located near the first-order mode (261.83 Hz) and the second-order mode (293.22 Hz), indicating that the excitation of the first two order modes will mainly produce transverse displacement. In Figure 14b, it can be seen that the resonance peaks of the bolts in the vertical direction of the three positions are all in the third-order mode (313.73 Hz), which can be summarized as follows: the first- and second-order modes mainly produce transverse acceleration, and the third-order mode mainly produces vertical acceleration.

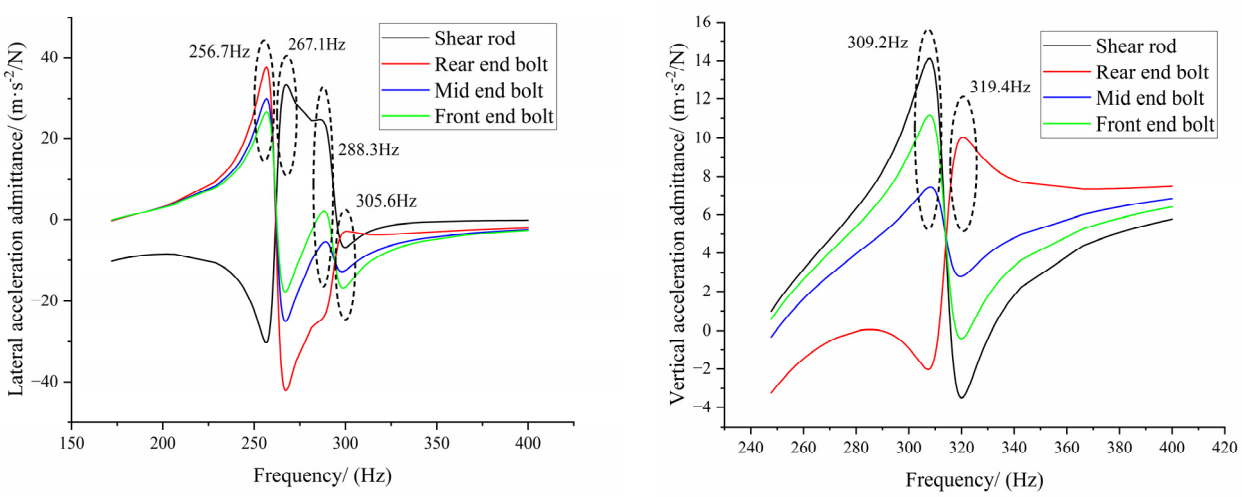

(**a**) (**b**)

Figure 14. Results of frequency-response analysis of the TMSH installed on the rubber pad in the vertical and lateral directions: (**a**) lateral acceleration admittance; (**b**) vertical acceleration admittance.

The addition of rubber pads can isolate most of the high-frequency vibrations, but there are still some high frequencies that will be reduced due to the increase in the rubber pads, and they will fall into the higher region of the floating-slab excitation energy. Tables 9 and 10 show the response amplitudes of the easily damaged areas of the TMSH (shear rod, front-end bolt, mid-end bolt, rear-end bolt) in the higher region of floating-slab excitation energy of 400–3000 Hz under the two structures with metal pads and rubber pads.

Table 9. Comparison of the magnitudes of the frequency responses of the TMSHs placed on the metal pad and the rubber pad under lateral excitation.

Work Conditions	Shear Rod	Rear-End Bolt	Mid-End Bolt	Front-End Bolt
Metal pad/dB	161.29	129.54	122.28	134.32
Rubber pad/dB	101.58	95.56	87.96	87.23
Improvement value/dB	59.71	33.98	34.32	47.09

The rubber pad has strong vibration isolation performance and can greatly reduce the vibration amplitude. In Table 8, we can see that the transverse vibration amplitude of each easily damaged part was reduced by more than 30 dB, among which the transverse vibration energy of the shear rod was attenuated by 59.71 dB. This proves that the rubber pad can effectively reduce the problem of shear-rod fracture while suppressing the problems of bolt loosening and broken bolts.

Table 10. Comparison of the magnitudes of the frequency responses of the TMSHs placed on the metal pad and the rubber pad under vertical excitation.

Work Conditions	Shear Rod	Rear-End Bolt	Mid-End Bolt	Front-End Bolt
Metal pad/dB	162.29	110.63	105.58	124.60
Rubber pad/dB	114.32	113.56	114.50	119.32
Improvement value/dB	47.97	−2.93	−8.92	5.28

5. Installation Modal Testing

Verification of the accuracy of numerical models is one of the main applications of experimental modal testing [35]. In particular, there is no precedent reference for this study, so it is necessary to conduct modal tests using the hammering method on the TMSH in its installed state to determine its natural frequency and vibration pattern.

5.1. Modal Test Principle

The basic idea of the modal test is to first establish a multi-degree-of-freedom dynamic ordinary differential equation, obtain the transfer function through its pull-type variation, and determine whether the transfer function contains the information of the modal parameters.

The differential equation of the system with N degrees of freedom after the structure has been discretized is:

$$[M]\ddot{X} + [C]\dot{X} + [K]X = F \tag{11}$$

where $[M]$ is the mass matrix; $[C]$ is the damping matrix; $[K]$ is the stiffness matrix; $\ddot{X}$, $\dot{X}$, and X represent the acceleration vector, velocity vector, and displacement vector of each discrete mass point in the system, respectively; and F represents the excitation-force vector.

In order to obtain the solution of the differential equation, a pull-type transformation of Equation (11) is performed, which yields:

$$[M]\left[s^2X(s) - sX(0) - \dot{X}(0)\right] + C(sX(s) - X(0)) + KX(s) = F(s) \tag{12}$$

When the initial conditions are all zero, the above equation changes to:

$$\left(s^2[M] + s[C] + [K]\right)X(s) = F(s) \tag{13}$$

According to the definition of a transfer function, the transfer function of the system is:

$$[H(s)] = \frac{1}{s^2[M] + s[C] + [K]} \tag{14}$$

Using the orthogonality of the matrix, when the modal matrix vibration is $[\varphi]$, the modal mass matrix, modal damping matrix, and modal stiffness matrix are:

$$[M]_r = [\varphi]^T[M][\varphi] = diag(m_1, \cdots, m_r, \cdots, m_N) \tag{15}$$

$$[C]_r = [\varphi]^T[C][\varphi] = diag(c_1, \cdots, c_r, \cdots, c_N) \tag{16}$$

$$[K]_r = [\varphi]^T[K][\varphi] = diag(k_1, \cdots, k_r, \cdots, k_N) \tag{17}$$

By substituting the above equation into the transfer function, we obtain:

$$[H(s)] = [\varphi]\left[s^2M_r + sC_r + K_r\right]^{-1}[\varphi]^T \tag{18}$$

Expanding the transfer function matrix reveals that each row or column contains the following basic modal information: all the elements of the modal mass matrix, modal damping matrix, modal stiffness matrix, and all modal vectors.

5.2. Modal Test under Installed Conditions

For this modal test, the Eastern Institute INV-3018 synchronous acquisition card was used due to the finite-element calculation results of the modal frequency being high. To ensure that the modal test did not lose order, we selected two ranges of 50 g and a range of 100 g for the PCB acceleration sensor via external tooling to form three acceleration sensors (the specific parameters are shown in Table 11). We used multi-point excitation and multi-point response (MIMO) with 2 preset response points and 67 excitation points. The shear hinge's natural frequency of concern was concentrated in the middle-to-high range, and a metal hammer head was used to generate pulse excitation.

Table 11. Sensor parameters.

Name	Sensitivity (mv/g)	Frequency Range Hz
PCB 352C33/ICP	100	0.5–10,000 Hz
PCB 353B31/ICP	50	1–5000 Hz

Due to the limitation of the test conditions, the modal test was carried out indoors, and a standard C55 concrete test block and rubber pad were used to simulate the FST to imitate actual floating-slab working conditions. According to [4], in a floating-slab structure that does not consider the subway train load, the FST's natural frequency should comply with the following formula:

$$f_0 = \frac{1}{2\pi}\sqrt{\frac{k_f}{m_f}} \tag{19}$$

where:

f_0 is the floating slab's natural frequency (Hz);

k_f is the floating slab's support stiffness per linear meter (N/m);

m_f is the mass of the floating slab per linear meter (kg).

The floating slab is mainly excited by the train load from the vertical direction during operation, and the support stiffness mentioned in the formula is understood as vertical stiffness. The first-order natural frequency of the prefabricated floating slab is about 13 Hz [36]. Considering the space limitation of the test chamber and the size of the shear hinge, the planned size of the cast concrete support was 0.5 m × 0.3 m × 0.18 m, its density was 2490 kg/m^3, and its calculated mass was 67.23 kg. Substituting these values into Equation (19) gives k_f = 448,548.65 Hz.

According to the formula for the rubber pad vertical stiffness (see Section 2.4), considering the stability of the concrete support and to ensure that the natural frequency was close to that of a real floating slab, four circular rubber pads were used for support. The principle was the same as that for four springs in parallel, so each rubber pad's vertical stiffness was required to be 112,137.16 Hz, which was substituted into the specific parameters of Formula (2) (see Table 12). The formula has two unknowns at the same time: the thickness of the rubber t_r and the rubber pad diameter D. These have an obvious positive relationship with the vertical stiffness, but through MATLAB R2022b software analysis, it was found that an increase in both of these factors at the same time will increase K_v. In order to obtain the target vertical stiffness and ensure that it is in line with the actual value, we assumed that t_r and D were 30 mm, 40 mm, and 50 mm at vertical stiffness values of 134,120 N/m, 178,820 N/m, and 223,530 N/m, respectively. Obviously, with a thickness of 30 mm, when the vertical stiffness is closer to the target value, the thickness cannot be greater than the diameter, or the support will be unstable. Therefore, the diameter was reduced and calculated using Formulas (2)–(4). Finally, for each rubber pad, we assumed that D = 28 mm and t_r = 30 mm.

Table 12. Calculated parameters of vertical stiffness of rubber pad.

IRHD	E_0/MPa	κ	E_∞/MPa	n
60	5.34	0.57	1150	1

Before the test, the TMSH was fixed with M24 bolts to a concrete base supported by four rubber pads, and two–three sensors were glued to measurement points 9 and 40 and connected to the acquisition card using BNC cables. The test system was set up as shown in Figure 15.

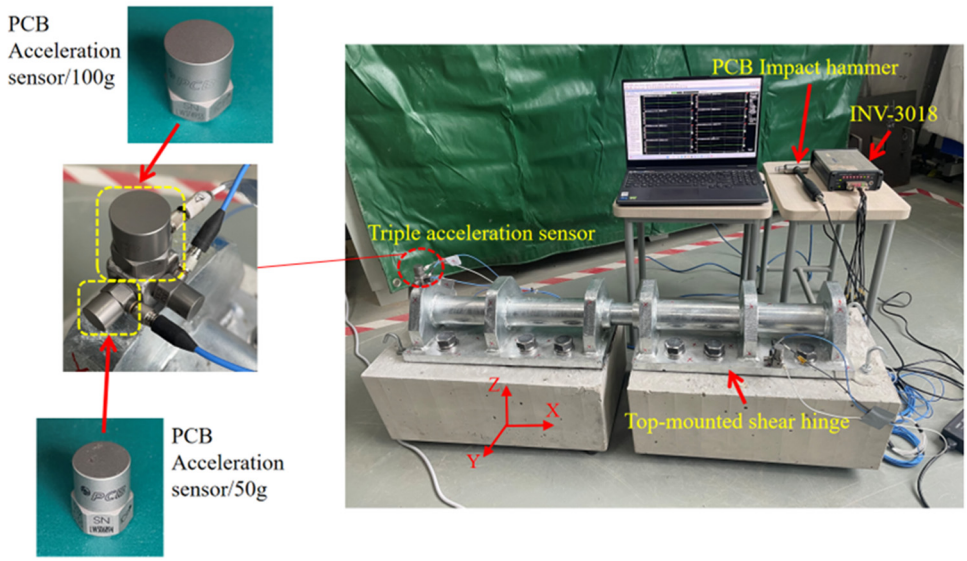

Figure 15. Indoor TMSH modal test.

The natural frequencies and vibration patterns obtained through the modal test of the percussion method were compared with the natural frequencies and vibration patterns obtained through the simulation (we used the metal pad case as an example of bending vibration pattern, and the rubber pad case as an example of the latter two orders of vibration pattern), as shown in Tables 13 and 14.

Table 13. Comparison of experimental and simulated modalities when TMSHs are installed on metal pads.

Mode Order	Experimental Mode/Hz	Experimental Nephogram	Simulation Mode/Hz	Simulation Nephogram	Error
1	1763.5	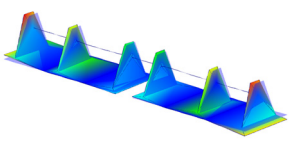	1947.4	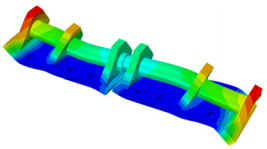	9.4%
2	2022.6	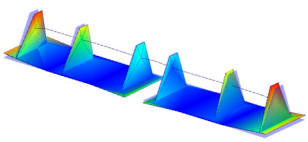	2248.8	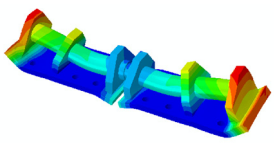	10%

Table 13. *Cont.*

Mode Order	Experimental Mode/Hz	Experimental Nephogram	Simulation Mode/Hz	Simulation Nephogram	Error
7	2681.0		2744.1		2.2%
8	2998.6		2808.9		6.3%

Table 14. Comparison of experimental and simulated modalities when TMSHs are installed on rubber pads.

Mode Order	Experimental Mode/Hz	Experimental Nephogram	Simulation Mode/Hz	Simulation Nephogram	Error
2	301.5		293.2		2.8%
3	325.2		313.7		3.5%

From the comparison, it was found that the difference between the natural frequencies in the test and simulation was within 10%, with a maximum error of 10% and a minimum error of 2.2%, which proves that the simulation results have a high degree of confidence. As shown in Figure 16, there was a linear relationship between the fifth-order mode and sixth-order mode, seventh-order mode, and eighth-order mode when the TMSH was installed on the metal pad, but this had little effect on the overall results.

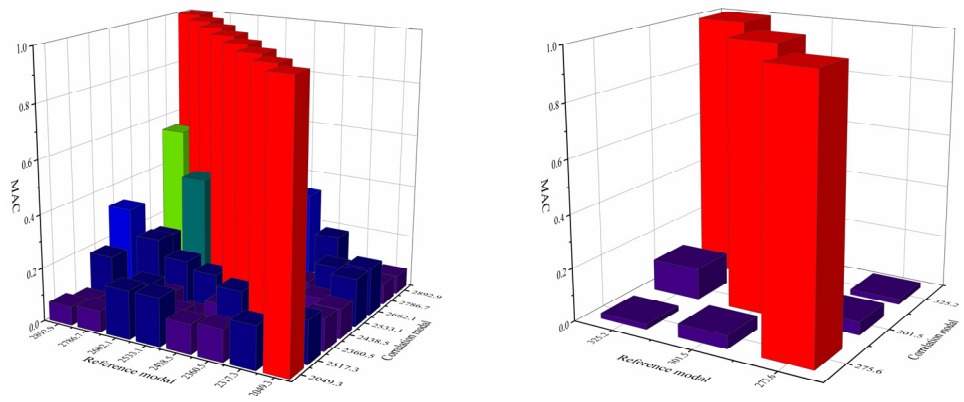

(**a**) (**b**)

Figure 16. Modal confidence criterion calibration (MAC) for modal test using the hammering method: (**a**) TMSH on the metal pad; (**b**) TMSH on the rubber pad.

6. Conclusions

To address the problem of damage to TMSHs under long-term train loads, a field investigation was conducted on an old and a new SSFST line. A refined model of the TMSH was established for dynamic characteristic analysis, and the simulation results were verified via indoor hammering tests on both structures. The following conclusions were obtained:

1. Through field research, it was determined that the main damage to the top-mounted shear hinges was mainly characterized by shear-rod fracture, bolt loosening, and broken bolts. Among these, bolt loosening was common in both the new and old lines and the curved section had more damage compared to the straight section. Based on rubber-damping theory, a new structure was formed by adding rubber mats between the shear-hinge structure and the metal pad. It is expected that the service life will be extended by reducing the shear hinge's natural frequency so that the natural frequency is located in the region of a lower vibration level of the floating-slab excitation, while also reducing the vibration amplitude in the higher part of the floating-slab excitation in the range of 400–3000 Hz.
2. By establishing a refined FEM of the SSFST and a refined model of the TMSH, the strength of the TMSH structure after the addition of the rubber pad was verified to be adequate. The pre-stress modal analysis of the TMSH assembly proved that the second-, third-, and seventh-order modes were the main causes of shear-rod fracture, and the reduced pre-stressing force under the third- and fifth-order modes of transverse vibration caused the bolts to loosen.
3. Upon comparing the vibration levels of the TMSH structure before adding the rubber pad and after adding the rubber pad under four different working conditions, it was found that, except for the linear section, the vibration level caused by floating-slab excitation can be effectively reduced in the curved section. It was reduced by eight times in the 4.8 m curved section and by at least three times in the 3.6 m curved section. Therefore, it is tentatively believed that adding rubber padding to the curved section can effectively extend the service life of the TMSH.
4. After adding the rubber pad, some natural frequencies higher than 3000 Hz were reduced to 400–3000 Hz in the high-vibration area of the floating slab. Due to the damping effect of the rubber pad, the transverse vibration amplitude of the easily damaged parts was reduced by more than 30 dB. Additionally, the transverse vibration energy of the shear rod was attenuated by 59.71 dB, the vertical vibration amplitudes of the rear-end bolt and mid-end bolt were slightly increased, and the vertical vibration amplitudes of the shear rod and the front-end bolt were reduced by 47.97 dB and 5.28 dB, respectively. It has been proven that the rubber pad can effectively reduce the problems of shear-hinge fracture, bolt loosening, and broken bolts.
5. The old and new TMSH structures were tested indoors using hammering tests to assess their modalities and validate the two simulation models separately. It was finally demonstrated, from both the test and simulation perspectives, that the new structure can effectively reduce the vibration amplitude of TMSHs when resonance occurs at the excited intrinsic frequency, thus delaying the occurrence of damage.

Discussion: This study innovatively analyzed the causes of damage to TMSHs (which have not been investigated in any of the current published literature). In order to reduce the occurrence of damage, a new type of TMSH was designed according to modal theory and the principle of damping using rubber pads. Through tests and simulations, it was proven that, after adding a rubber pad, the natural frequency of the TMSH decreased to that of the low-vibration region of the floating slab. However, because the natural frequency of the TMSH is generally high, some of the natural frequencies decreased to that of the high-vibration region of the floating slab, and the vibration isolation of the rubber pad reduced the vibration amplitude of the TMSH, which is located in the high-vibration region of the floating slab. Extending the life of the TMSH also reduces the chances of damage to floating-slab joint fasteners and steel springs, thereby increasing the overall stiffness and

traveling stability of the line. The next step will be to apply this new TMSH in the field, examine its practicality, and investigate the use of materials other than rubber, or the use of different rubber-pad shapes, to replace the ring-shaped rubber pads.

Author Contributions: Conceptualization, A.W.; methodology, A.W.; software, H.E.; formal analysis, H.E.; investigation, H.E.; resources, Y.H.; writing—original draft preparation, H.E.; writing—review and editing, H.E.; visualization, H.E.; supervision, A.W. and Y.H.; project administration, H.L.; funding acquisition, Y.H. All authors have read and agreed to the published version of the manuscript.

Funding: This research was funded by "Chaotic Dynamics of Ballast Bed Damage in High-Speed Railways" of the National Natural Science Foundation of China (51978393), and "Online Monitoring and Analysis Technology for Fasteners and Key Vibration Isolation Units" of the Shanghai Science and Technology Innovation Action Plan for Social Development in 2020 (20dz1203104). The above support is greatly appreciated.

Institutional Review Board Statement: Not applicable.

Informed Consent Statement: Not applicable.

Data Availability Statement: Not applicable.

Conflicts of Interest: The authors declare no conflict of interest.

References

1. Saurenman, H.; Phillips, J. In-Service Tests of the Effectiveness of Vibration Control Measures on the BART Rail Transit System. *J. Sound Vib.* **2006**, *293*, 888–900. [CrossRef]
2. Wang, A.; Cox, S.J.; Huang, H.; Liu, L.; Jiang, J.; Sun, J. In-Car Noise and Carriage Floor Vibration on Different Track Forms and Curvatures in a Metro System. In *Noise and Vibration Mitigation for Rail Transportation Systems*; Schulte-Werning, B., Thompson, D., Gautier, P.-E., Hanson, C., Hemsworth, B., Nelson, J., Maeda, T., Vos, P., Eds.; Notes on Numerical Fluid Mechanics and Multidisciplinary Design; Springer: Berlin/Heidelberg, Germany, 2008; Volume 99, pp. 201–207, ISBN 978-3-540-74892-2.
3. Huang, X.; Zeng, Z.; Wang, D.; Luo, X.; Li, P.; Wang, W. Experimental Study on the Vibration Reduction Characteristics of the Floating Slab Track for 160 Km/h Urban Rail Transit. *Structures* **2023**, *51*, 1230–1244. [CrossRef]
4. *CJJ/T 191-2012*; Technical Specifications for Floating Slab Tracks. Ministry of Housing and Urban-Rural Development of the People's Republic of China: Beijing, China, 2012. (In Chinese)
5. Zhao, C.; Liu, D.; Zhang, X.; Yi, Q.; Wang, L.; Wang, P. Influence of Vibration Isolator Failure on Vehicle Operation Performance and Floating Slab Track Structure Vibration Reduction Effectiveness. *Shock Vib.* **2019**, *2019*, 1–14. [CrossRef]
6. Xiao, X.; Jin, X.; Wen, Z. Effect of Track Support Failure on Dynamic Response of Tangent Track. *Lixue Xuebao Chin. J. Theor. Appl. Mech.* **2008**, *40*, 67–78.
7. Zhan, T.; Yao, Y.; Li, J.; Liu, X.; Feng, Y. Influence of Fastener Failure on Dynamic Performance of Subway Vehicle. *Appl. Sci.* **2022**, *12*, 6769. [CrossRef]
8. Xu, L.; Gao, J.; Zhai, W. On Effects of Rail Fastener Failure on Vehicle/Track Interactions. *Struct. Eng. Mech.* **2017**, *63*, 659–667. [CrossRef]
9. Li, Q.; Wang, F.; Wang, Y.; Zhou, C.; Chen, J.; Forson, K.; Miao, R.; Su, Y.; Zhang, J. Effect of Reservoir Characteristics and Chemicals on Filtration Property of Water-Based Drilling Fluid in Unconventional Reservoir and Mechanism Disclosure. *Environ. Sci. Pollut. Res.* **2023**, *30*, 55034–55043. [CrossRef]
10. Li, T.; Qin, A.; Pei, Y.; Sun, D.; Fu, X. Semianalytical Solutions to the Consolidation of Drainage Well Foundations in Unsaturated Soils with Radial Semipermeable Drainage Boundary under Time-Dependent Loading. *Int. J. Geomech.* **2020**, *20*, 04020150. [CrossRef]
11. Wang, F.; Liu, X.; Jiang, B.; Zhuo, H.; Chen, W.; Chen, Y.; Li, X. Low-Loading Pt Nanoparticles Combined with the Atomically Dispersed FeN4 Sites Supported by FeSA-N-C for Improved Activity and Stability towards Oxygen Reduction Reaction/Hydrogen Evolution Reaction in Acid and Alkaline Media. *J. Colloid Interface Sci.* **2023**, *635*, 514–523. [CrossRef]
12. Chung, W.; Kwon, K.; Jang, S.Y. Deflection-Based Load Transfer Efficiency of Floating Slab Track. *KSCE J. Civ. Eng.* **2014**, *18*, 616–624. [CrossRef]
13. Hussein, M.; Alves Costa, P. The Effect of End Bearings on the Dynamic Behaviour of Floating-Slab Tracks with Discrete Slab Units. *Int. J. Rail Transp.* **2016**, *5*, 38–49. [CrossRef]
14. Xu, Q.; Yan, B.; Lou, P.; Zhou, X. Influence of Slab Length on Dynamic Characteristics of Subway Train-Steel Spring Floating Slab Track-Tunnel Coupled System. *Lat. Am. J. Solids Struct.* **2015**, *12*, 649–674. [CrossRef]
15. Xu, Q.; Xiao, Z.; Liu, T.; Lou, P.; Song, X. Comparison of 2D and 3D Prediction Models for Environmental Vibration Induced by Underground Railway with Two Types of Tracks. *Comput. Geotech.* **2015**, *68*, 169–183. [CrossRef]
16. Wei, G.; Wang, Y.-A.; Jiang, J.-Q.; Zhang, R.; Ding, Z. Effect of Dowel Joints on Dynamic Behavior of Train–Discrete Floating Slab Track System. *Adv. Mech. Eng.* **2018**, *10*, 168781401876701. [CrossRef]

17. Ma, D.; Shi, J.; Yan, Z.; Xiao, J.; Sun, L. Experimental and Numerical Investigation of the Effect of the Assembled State on the Static-Dynamic Characteristics and Fatigue Performance of Railway Fastening Clips. *Structures* **2022**, *46*, 1808–1822. [CrossRef]
18. Xiao, H.; Wang, J.-B.; Zhang, Y.-R. The Fractures of E-Type Fastening Clips Used in the Subway: Theory and Experiment. *Eng. Fail. Anal.* **2017**, *81*, 57–68. [CrossRef]
19. Gao, X.; Wang, A.; Liu, L.; He, Y.; Ju, L. Analysis of Failure Mechanism of W1-Type Fastening Clip in High Speed Railway and Structure Study of Damping Composite. *Eng. Fail. Anal.* **2020**, *118*, 104848. [CrossRef]
20. Dai, W.; Moroni, M.O.; Roesset, J.M.; Sarrazin, M. Effect of Isolation Pads and Their Stiffness on the Dynamic Characteristics of Bridges. *Eng. Struct.* **2006**, *28*, 1298–1306. [CrossRef]
21. Xin, T.; Ding, Y.; Wang, P.; Gao, L. Application of Rubber Mats in Transition Zone between Two Different Slab Tracks in High-Speed Railway. *Constr. Build. Mater.* **2020**, *243*, 118219. [CrossRef]
22. Liu, T.; Rao, R.; Liu, J.; Ye, M.; Huang, Y. Experimental Study on the Damping Effects of Various Vibration Reduction Measures. *IOP Conf. Ser. Mater. Sci. Eng.* **2020**, *735*, 012067. [CrossRef]
23. Jin, H.; Zhou, S.; Liu, W. Optimization of Vibration Reduction of the Rubber Floating-Slab Tracks. *J. Vibroeng.* **2017**, *19*, 1214–1224. [CrossRef]
24. Jin, H.; Liu, W.; Zhou, S. An Experiment to Assess Vibration Reduction Ability of the Rubber Floating-Slab Tracks with Different Supporting Forms. *J. Vibroeng.* **2015**, *17*, 3237–3246.
25. Luo, R.K.; Mortel, W.J.; Wu, X.; Peng, L.M. Evaluation of Stress Softening of the Rubber Suspension Used on Rail Vehicles. *Proc. Inst. Mech. Eng. Part F J. Rail Rapid Transit* **2016**, *230*, 15–23. [CrossRef]
26. Zhao, C.; Shi, D.; Zheng, J.; Niu, Y.; Wang, P. New Floating Slab Track Isolator for Vibration Reduction Using Particle Damping Vibration Absorption and Bandgap Vibration Resistance. *Constr. Build. Mater.* **2022**, *336*, 127561. [CrossRef]
27. Liu, W.; Miyama, T.; Feng, D.; Zhou, F. Simplified Calculation Method for Vertical Stiffness of Rubber Isolation Bearings. *Earthq. Eng. Eng. Vib.* **2001**, *21*, 111–116. (In Chinese) [CrossRef]
28. *GB 20688.3-2006*; Rubber bearings—Part 3: Rubber bearings for seismic isolation of buildings. General Administration of Quality Supervision, Inspection and Quarantine of the People's Republic of China: Beijing, China, 2006. (In Chinese)
29. Huang, X.; Zeng, Z.; Li, Z.; Wang, W.; Yuan, Y.; Yuan, W.; Boumedienne, H.S. Comparative Research on Vibration Characteristics of Cast-In-Place Steel-Spring-Floating Slab Track under Different Subway Line Conditions. *Appl. Sci.* **2022**, *12*, 5079. [CrossRef]
30. Tang, M.-Z.; Xiong, X.-H.; Li, X.-B.; Chen, G.; Zhang, J.; Zhong, M.; Sun, B. Dynamic Response of Outer Windshield Structure in Different Schemes under Aerodynamic Load. *Appl. Sci.* **2023**, *13*, 3879. [CrossRef]
31. Jiang, C.; Xiong, W.; Cai, C.S.; Zhu, Y.; Wang, J. Preload Loss of High-Strength Bolts in Friction Connections Considering Corrosion Damage and Fatigue Loading. *Eng. Fail. Anal.* **2022**, *137*, 106416. [CrossRef]
32. Wang, Y.-Z.; Li, G.-Q.; Wang, Y.-B.; Lyu, Y.-F. Simplified Method to Identify Full von Mises Stress-Strain Curve of Structural Metals. *J. Constr. Steel Res.* **2021**, *181*, 106624. [CrossRef]
33. *TB/T 10082-2005*; Railway Track Design Specifications. National Railway Administration of the People's Republic of China: Beijing, China, 2005. (In Chinese)
34. Zeng, Z.; Huang, X.; Li, Z.; Wang, W.; Shi, Z.; Yuan, Y.; Shuaibu, A.A. Experimental Research on Vibration-Damping Effect of Combined Shear Hinge Prefabricated Steel Spring Floating Slab Track. *Sensors* **2022**, *22*, 2567. [CrossRef]
35. Luczak, M.M.; Riva, R.; Yeniceli, S.C.; Madsen, S.H.; Di Lorenzo, E. Identification of the Test Setup Influence on the Modal Properties of a Short Wind Turbine Blade during Fatigue Test. *Measurement* **2021**, *174*, 108960. [CrossRef]
36. Lei, X.; Jiang, C. Analysis of Vibration Reduction Effect of Steel Spring Floating Slab Track with Finite Elements. *J. Vib. Control* **2016**, *22*, 1462–1471. [CrossRef]

Disclaimer/Publisher's Note: The statements, opinions and data contained in all publications are solely those of the individual author(s) and contributor(s) and not of MDPI and/or the editor(s). MDPI and/or the editor(s) disclaim responsibility for any injury to people or property resulting from any ideas, methods, instructions or products referred to in the content.